Electronic structure and localization of electron density at the Ca/GaN(0001) monolayer interface

© M.N. Lapushkin

Ioffe Institute,
194021 St. Petersburg, Russia
E-mail: Lapushkin@ms.ioffe.ru

Received June 17, 2026
Revised August 14, 2026
Accepted August 20, 2026

The adsorption of calcium atoms on the GaN(0001) surface was studied using the density functional method. GaN(0001) was modeled as a 2×2GaN(0001) supercell containing 10 GaN bilayers. With a monolayer coverage of calcium, Ca atoms are adsorbed above the surface N atoms. A zone of surface states of calcium is formed near the Fermi level. The interaction of calcium valence electrons with electrons of Ga dangling bonds leads to charge localization in the region of the Ca–Ga bond.

Keywords: gallium nitride, calcium, adsorption, electronic structure.

DOI: 10.61011/SC.2026.05.63997.10235

1. Introduction

Gallium nitride (GaN) heterostructures are widely used because of their distinctive physical properties. GaN is a wide-band-gap semiconductor; together with its high thermal conductivity, thermal stability, and strong light emission, this makes it an essential material for modern electronics [1]. GaN is currently used extensively in high-power semiconductor devices [2] and various types of light-emitting diodes [3]. Modifying GaN surfaces by depositing or implanting atoms, particularly metals, enables targeted changes in their physicochemical and electronic properties. This opens opportunities for various GaN-based devices, including high-efficiency sensors and catalysts.

Adsorption of various atoms and molecules on GaN(0001) has been studied in numerous experiments and calculations, summarized in Ref. [4]. Magnesium doping is most commonly used to obtain *p*-type GaN: Mg atoms substitute for Ga atoms, creating acceptor levels. It is therefore important to investigate how other alkaline earth elements affect the electronic properties of gallium nitride and assess their potential as alternative dopants. Here calcium adsorption on GaN(0001) is modeled using density functional theory.

Studies of alkaline earth metal adsorption on GaN(0001) have traditionally focused on Mg. Experimental data on calcium deposition are currently absent from the literature. Barium and magnesium adsorption on gallium nitride has, however, been studied extensively in experiments [4]. Barium adsorption on Ga-polar GaN(0001) was investigated at submonolayer coverages by photoemission excited with visible light and synchrotron radiation [5,6]. The authors attributed the photoemission spectra to excitation of a two-dimensional accumulation layer near the Fermi level. In addition, visible-light photoemission (in the transparency region of gallium nitride) exhibited photocurrent oscillations caused by interference within the GaN film. Reference [7] examined the growth, structure, and electronic properties of thin (≤ 20 Å) Mg films on GaN(0001) by Auger electron spectroscopy, photoemission, and low-energy electron diffraction. Epitaxial growth at room temperature produced a metallic layer. Mg and Ga exchanged sites, incorporating Mg into GaN near the interface. In contrast, Ref. [8] reported Stranski–Krastanov growth of the magnesium layer. Density functional calculations examined Mg monolayer adsorption on Ga-polar GaN(0001) using a $2 \times 2 \times 10$ supercell. An unconventional mixed configuration, with Mg atoms above N atoms and at bridge sites between N atoms, was energetically preferred, with an adsorption energy of -1.175 eV. Only minor substrate reconstruction was found, together with formation of a broad surface band below the Fermi level through interaction of the valence electrons of magnesium and GaN.

Only a limited number of publications model alkaline earth adsorption on Ga-polar GaN(0001). Some focus on the mechanisms of Mg incorporation into the semiconductor substrate. Other studies describe magnesium deposition on a graphene-like monolayer (*g*-GaN). For example, the authors of Ref. [9] used density functional theory for quantum-chemical calculations of alkaline earth metal interactions (including Ca) with *g*-GaN. Their model employed a 3×3 supercell containing 18 atoms. At a coverage of 1/18 monolayer (ML), calcium preferentially occupied sites above Ga atoms, with a calculated adsorption energy (E_{ads}) of -4.17 eV. The Ca surface-state band peaked 3 eV below the Fermi level, within the *g*-GaN valence band. The calculated optical absorption coefficient had several peaks between 1.5 and 2.9 eV, suggesting potential use of these systems for visible-light-driven catalytic processes. Reference [10] used density functional theory to calculate Be and Ca adsorption on *g*-GaN monolayers, with one adatom in 2×2, 3×3, and 4×4 supercells. The magnitude

of the Ca adsorption energy decreased with increasing coverage, from -3.08 to -2.62 eV. At these coverages, g-GaN retained its semiconductor character. A broad band of electronic states formed below the Fermi level between -3.5 and -1.5 eV, with a narrow peak just below the Fermi level. Electron density was transferred from calcium to g-GaN. With increasing calcium coverage, the transferred charge decreased from $0.85e$ to $0.75e$. References [11,12] investigated photoluminescence from Ca-implanted GaN. The PL peak was at 2.5 eV, exceeding the theoretical value by 0.27 eV, and was shown to be associated with Ca_{Ga} acceptors.

Ca is a candidate for replacing Li in ion batteries [10,13]. It can also act as a nonradiative recombination center in GaN, adversely affecting the efficiency of III-nitride light-emitting diodes [11]. An adsorbed monolayer can be regarded as the first stage in metal–semiconductor interface formation. As the review shows, virtually no calculations address monolayer coverage of GaN with alkaline earth atoms; existing studies instead consider a single atom adsorbed on a supercell surface to reduce computational time. The literature also lacks information on the relationship between the size of an adsorbed alkaline earth atom and the spatial distribution of preferred adsorption sites during monolayer formation on III-nitride surfaces. Calculations of an Mg monolayer on GaN(0001) [14] showed an unconventional adsorption configuration: magnesium atoms form a 3.216×2.592 Å rectangle, with two sites above N atoms (T_N) and two bridge sites between N atoms. It is therefore necessary to establish whether this configuration is unique or characteristic of other alkaline earth adsorbates. Adsorption studies determine both the adsorption sites and energies, providing a basis for subsequent investigation of atom diffusion into the substrate, i.e., substrate doping.

The effect of Ca atoms on Ga-polar GaN(0001) has not previously been studied. The aim of this work is quantum-mechanical modeling of Ca adsorption on GaN(0001) to determine how adsorbed Ca affects the surface electronic properties. Specifically, we determine the energetically preferred adsorption site, adsorption energy, surface electronic structure, and electron density localization induced by a calcium monolayer.

The problem is addressed within density functional theory (DFT), using the local density approximation (LDA) for exchange and correlation [15]. The choice of LDA is also motivated by the availability of pseudo-hydrogen pseudopotentials developed for this functional in open databases. Despite its long history and known limitations, LDA remains relevant to current research [16–18]. Its principal advantages are relatively low computational cost and high speed compared with hybrid functionals. This allows efficient treatment of supercells containing many atoms. A fundamental limitation of DFT calculations is systematic underestimation of semiconductor band gaps E_g, by up to 50 % [19–21]. The most accurate E_g values are obtained using hybrid functionals such as HSE [22]. For GaN, HSE [23] gives $E_g = 3.51$ eV, in good agreement with the experimental value of 3.4 eV. However, calculations with HSE-family functionals require an order of magnitude more computing time than conventional exchange-correlation schemes. Various approaches are used to correct the band-gap error, including conduction band shifts (scissoring operator) [24], Hubbard corrections (DFT+U) [25], the modified Becke–Johnson functional (mBJ) [26], and LDA1/2 [27].

2. Computational details

The atomic and electronic structures were modeled using density functional theory (DFT). Calculations were performed with Quantum Espresso [28], with exchange and correlation described by the local density approximation (LDA) [15] and ultrasoft pseudopotentials. Gaussian smearing with a width of 0.01 Ry (Rydberg) was used. Slabs were separated by a 52 Å vacuum layer to avoid unwanted interslab electric fields. The plane-wave basis had kinetic energy cutoffs of 45 Ry for wave functions and 406 Ry for electron density. Geometry relaxation used a γ-centered k-point mesh of $4 \times 4 \times 1$, while the final electronic structure calculation used a denser $8 \times 8 \times 1$ mesh.

GaN(0001) was modeled by a $2 \times 2 \times 10$ supercell (Figure 1). The unit-cell parameters were fixed. The values used were $a = b = 3.216$ Å and $c = 5.240$ Å, close to the experimental values $a = 3.22$ Å and $c = 5.23$ Å. The number of GaN bilayers was chosen to eliminate surface effects on the electronic structure of the central bilayers while providing an optimal balance between accuracy and computational cost. The bottom of the supercell was terminated by pseudo-hydrogen atoms with the recommended charge of $0.75e$ [29–31]. The surface GaN bilayer, adsorbate layer, and pseudo-H layer (for the clean surface only) were relaxed. Atoms in the remaining bilayers were fixed to

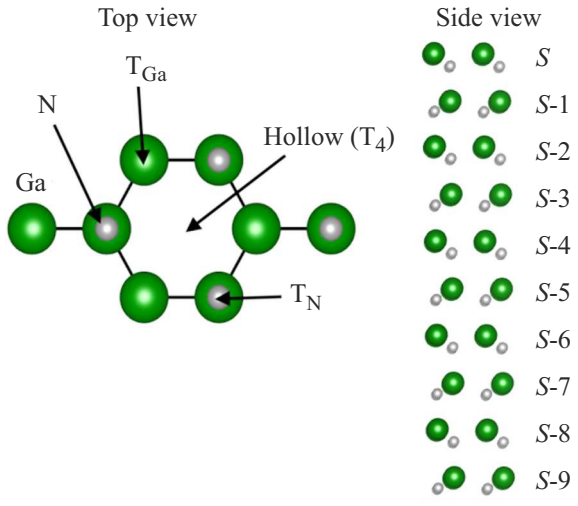


Figure 1. GaN(0001) supercell. Arrows indicate stable adsorption sites.

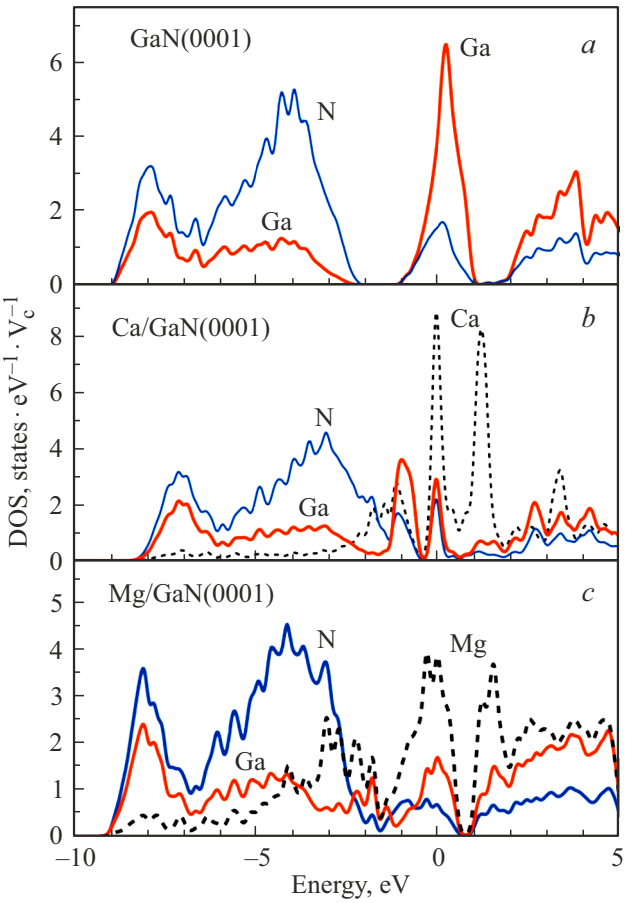


Figure 2. Partial density of states of the surface layer: GaN(0001) (*a*), Ca/GaN(0001) (*b*), and Mg/GaN(0001) (*c*) [31]. $E_F = 0$ eV. V_c is the unit-cell volume.

represent the bulk. Relaxation was terminated when the force magnitudes were below 10^{-4} Ry/Å.

3. Calculation results

The electronic density of states of the surface bilayer (*S*) of the clean, relaxed GaN(0001) surface is shown in Figure 2, *a*. The principal surface-state peak lies near the Fermi level at $E = 0.20$ eV, indicating surface metallization. Another broad peak above the Fermi level (E_F) has a maximum at 4.0 eV. These states arise predominantly from Ga 4*p*-orbitals, with a much smaller contribution from N 2*p*-orbitals. Figure 3, *a* shows the spatial electron density distribution of surface states in the energy range from -1.0 eV to E_F. The N 2*p*-states are more strongly localized and lie considerably farther from the surface plane than the Ga 4*p*-states.

In bilayer (*S*-1), the surface-state density at the Fermi level decreases by a factor of ~ 10. The surface influence on the electronic structure of deeper layers decays rapidly, becoming nearly bulk-like in bilayer (*S*-4). This agrees well with previous GaN calculations discussed in Ref. [7].

Ca adsorption parameters: binding energies and interplanar distances *h* from the surface gallium atoms

	E_{ads}, eV	*h*, Å
T_N	−1.698	2.32
T_{Ga}	−0.988	3.17
T_4 hollow site	−1.531	2.47

The adsorption energy (E_{ads}) per Ca adatom was calculated as

$$E_{ads} = \left(E_{GaN_Ca} - E_{GaN} - E_{Ca}\right)/4, \qquad (1)$$

where E_{GaN_Ca} and E_{GaN} are the total energies with and without adsorbed Ca, and E_{Ca} is the total energy of the Ca monolayer. The table lists calcium adsorption energies and the interplanar distances between the calcium layer and surface gallium atoms for different high-symmetry adsorption sites.

Adsorption at bridge sites between Ga and N atoms is energetically unfavorable. Ca atoms preferentially occupy T_N sites. This differs from Mg monolayer adsorption on GaN(0001) [14], where the magnesium atoms form an unconventional configuration, a 3.216×2.592 Å rectangle with two T_N sites and two bridge sites between N atoms. For a Ca monolayer, this initial configuration is unstable, and the atoms migrate to T_N. The difference

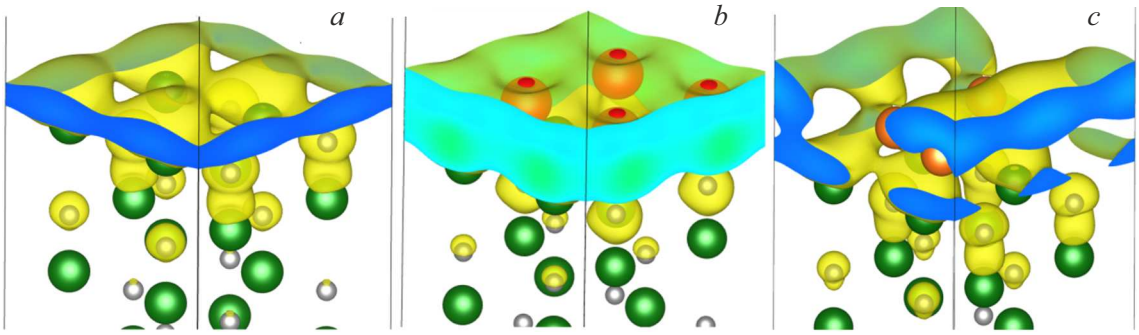


Figure 3. Partial charge density associated with occupied surface states of clean GaN(0001) (*a*) and after adsorption of a Ca (*b*) or Mg (*c*) monolayer. The saturation level is 0.0022 e/Å^3 (*a*), 0.0031 e/Å^3 (*b*), and 0.0019 e/Å^3 (*c*).

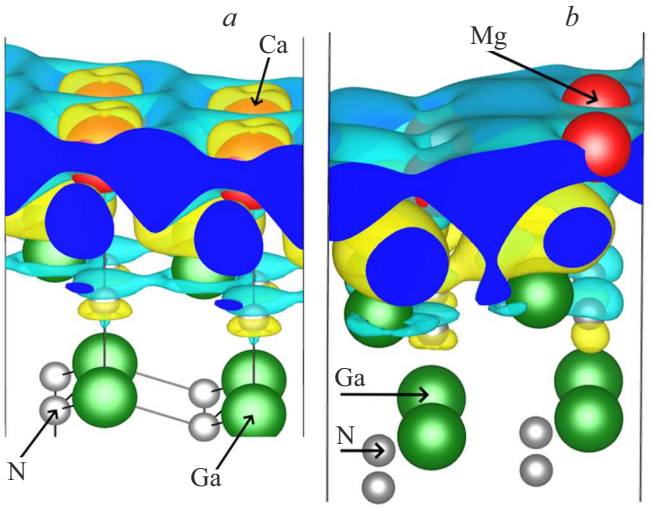


Figure 4. Electron density difference $\Delta\rho(r)$ after adsorption of a Ca (a) or Mg (b) monolayer. Light blue and yellow contours indicate charge depletion and accumulation regions, respectively. The blue line shows the $\delta\rho(r)$ profile along the boundary of the computational supercell.

may be related to the Mg and Ca atomic radii, 1.60 and 1.97 Å, respectively. At the same coverage, the calcium adsorption energy is larger in magnitude than that of magnesium ($E_{ads} = -1.175$ eV). The resulting magnitude is smaller than for 0.25 ML Ca coverage on g-GaN ($E_{ads} = -2.62$ eV) [10]. This difference mainly reflects the substrate type and coverage, and, to a lesser extent, the calculation method.

After Ca monolayer adsorption at T_N sites, the distance between the surface Ga and N atomic planes increases by 8 %. This is accompanied by a redistribution of the surface electronic density of states near E_F. Calcium surface-state bands form: a narrow band at the Fermi level and a broad band (~ 3 eV) peaking at -1.15 eV (Figure 2, b). These bands originate from hybridized Ca 4sp-states. The peak at E_F is predominantly due to Ca 4p-states, whereas the broad peak arises from Ca 4sp-states. The GaN surface-state peaks in the surface layer (Figure 2, b) split into two, at -1.03 and -0.04 eV. The effect of the adsorbed Ca layer on the electronic structure of GaN bilayers decreases rapidly with depth. In bilayer (S-1), the surface-state density falls sharply, by an order of magnitude. By bilayer (S-3), the calcium monolayer has no discernible effect on the electronic structure. The shift of the valence band edges of the surface (S) and central (S-4) GaN bilayers indicates that Ca monolayer adsorption induces upward band bending of ~ 0.3 eV. Calculations of Mg monolayer adsorption on GaN(0001) reported in Ref. [14] are qualitatively consistent with the present Ca results. Differences are also present (Figure 2, c), owing to the smaller atomic radius and higher ionization potential of Mg and its unconventional adsorption configuration. A broader peak at E_F is obtained. The results for the adsorbed Mg monolayer in Figs. 3–5 were calculated as part of the present work.

Figure 3, b shows the spatial electron density distribution of surface states between -1.0 eV and E_F after Ca monolayer adsorption. The N 2p-states become more spatially localized and do not participate in bonding to the adsorbates. The Ga 4p-states participate in bonding to the adsorbed atoms and are localized in the bond region. Similar results are obtained for an Mg monolayer (Figure 3, c), with differences due to the unconventional adsorption sites.

Calcium chemisorption on GaN(0001) arises from chemical bond formation through sharing of Ga and Ca valence electrons. The associated charge redistribution increases electron density locally in the Ga–Ca interstitial region, while depleting it near the Ca atom itself. This is clearly seen in Figure 4, a, showing the charge density difference $\Delta\rho(r)$ after Ca adsorption on GaN(0001).

Electron density $\rho(r)$ accumulates in the Ca–Ga bond region, owing to interaction with the dangling bonds of surface Ga atoms. By contrast, $\rho(r)$ is depleted in the

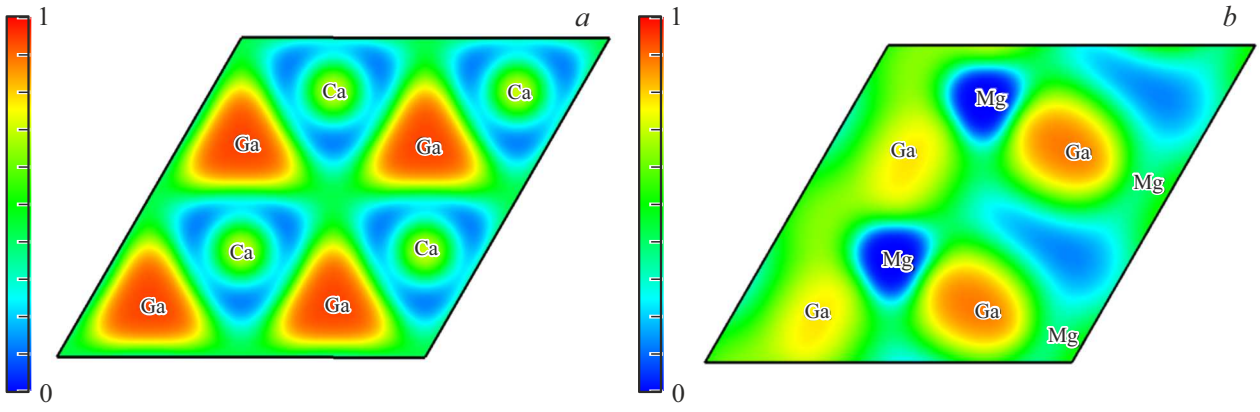


Figure 5. Electron localization function after adsorption of a Ca (a) or Mg (b) monolayer: top view. The section passes through the maximum ELF between the surface Ga atoms and adsorbed Ca(Mg) atoms. The section lies above the Ga atomic plane by 1.39 Å for the Ca monolayer and 1.54 Å for Mg.

Ca atomic plane. The interatomic electron density between Ga and N within the surface GaN bilayer changes only slightly.

Adsorbed Ca interacts with the GaN(0001) surface through chemical bonds between Ga and Ca valence electrons. Electron density increases in the Ga−Ca bond region, with a corresponding decrease near the Ca atom. A similar pattern is found for Mg adsorption (Figure 4, *b*).

The spatial distribution of the electron localization function (ELF) [32] upon Ca monolayer formation is visualized as a 2D section in Figure 5, *a*. This dimensionless quantity is constrained to values between 0 and 1. Values near the upper limit indicate strongly localized electron density in the corresponding region of space, whereas ELF = 0 indicates its virtual absence. ELF = 0.5 corresponds to complete electron delocalization, characteristic of a homogeneous electron gas. The maximum, ELF = 1, corresponds to ideally localized electron pairs.

For the calcium monolayer, the maximum is ELF = 0.95 (Figure 5, *a*). This indicates strong electron density localization in the Ca−Ga bond region. The results in Figure 4, *b* support the conclusions from the electron density difference analysis. The unconventional Mg adsorption configuration produces an asymmetric ELF distribution (Figure 5, *b*), with a slightly lower ELF = 0.88 and therefore slightly weaker electron localization. For the lower-lying Mg atoms, ELF = 0.85.

Comparing Mg and Ca adsorption on GaN(0001) shows the strong influence of adsorbate atomic size. This affects both adsorption sites and electron density localization at the interface.

4. Conclusion

Calculations of calcium monolayer adsorption on Ga-polar GaN(0001) identified the energetically preferred configuration. Calcium atoms preferentially adsorb at high-symmetry sites above nitrogen atoms. Ca monolayer adsorption induces spatial charge redistribution, with pronounced electron density transfer at the Ca/GaN(0001) interface and subsequent localization in the Ca−Ga bond region. Calcium-derived bands form near and below the Fermi level, and the GaN surface-state band is modified. Changes in the near-surface gallium nitride layer shift the valence band edge to lower energies, indicating upward band bending. Comparison of calcium and magnesium adsorption shows that atomic size affects adsorption sites and the electronic structure of the adsorbate/GaN(0001) interface.

Conflict of interest

The author declares that he has no conflict of interest.

References

[1] Z. Wang, G. Wang, X. Liu, S. Wang, T. Wang, S. Zhang, J. Yu, G. Zhao, L. Zhang. J. Mater. Chem. C, **9**, 17201 (2021). DOI: 10.1039/D1TC04022G

[2] R. Sun, J. Lai, W. Chen, B. Zhang. IEEE Access, **8**, 15529 (2020). DOI: 10.1109/ACCESS.2020.2967027

[3] M. Behringer, H. König. PhotonicsViews, **17**, 60 (2020). DOI:10.1002/phvs.202000018

[4] V.M. Bermudez. Surf. Sci. Rep., **72** (4), 147 (2017). DOI: 10.1016/j.surfrep.2017.05.001

[5] G.V. Benemanskaya, M.N. Lapushkin, S.N. Timoshnev. Surf. Sci., **603** (16), 2474 (2009). DOI: 10.1016/j.susc.2009.05.022

[6] G.V. Benemanskaya, S.N. Timoshnev, S.V. Ivanov, G.E. Frank-Kamenetskaya, D.E. Marchenko, G.N. Iluridze. J. Exp. Theor. Phys., **118** (4), 600 (2014). DOI: 10.1134/S1063776114040098

[7] V.M. Bermudes. Surf. Sci., **417**, 30 (1998). DOI: 10.1016/S0039-6028(98)00659-1

[8] Y. Yang, S. Mishra, F. Cerrina, S.H. Xu, H. Cruguel, G.J. Lapeyre, J.F. Schetzina. J. Vac. Sci. Technol. B, **17** (4), 1884 (1999). DOI: 10.1116/1.590840

[9] Z. Cui, X. Wang, M. Li, J. Zheng, Y. Ding, T. Liu. Solid State Commun., **296**, 26 (2019). DOI: 10.1016/j.ssc.2019.04.01

[10] K.H. Yeoh, T.L. Yoon, T.-L. Lim, Rusi, D.S. Ong. Superlat. Microstruct., **130**, 428 (2019). DOI: 10.1016/j.spmi.2019.05.011

[11] M.A. Reshchikov, D.O. Demchenko, M. Vorobiov, O. Andrieiev, B. McEwen, F. Shahedipour-Sandvik, K. Sierakowski, P. Jaroszynski, M. Bockowski. Phys. Rev. B, **106**, 035206 (2022). DOI: 10.1103/PhysRevB.106.035206

[12] M.A. Reshchikov. Phys. Status Solidi B, **260**, 2200488 (2023). DOI: 10.1002/pssb.202200488

[13] Y. Wu, Z. Zhao, X. Hao, R. Xu, L. Li, D. Lv, X. Huang, Q. Zhao, Y. Wu. Carbon Neutralization, **2**, 551 (2023). DOI: 10.1002/cnl2.85

[14] M.N. Lapushkin. Phys. and chem. aspects of the study of clusters, nanostructures and nanomaterials, **17**, 447 (2025). DOI: 10.26456/pcascnn/2025.17.447 (In Russian).

[15] J.P. Perdew, A. Zunger. Phys. Rev. B, **23**, (10), 5048 (1981). DOI: 10.1103/PhysRevB.23.5048

[16] L. Lymperakis, K. Lymperakis, E. Iliopoulos. J. Appl. Phys., **136** (21), 215701 (2024). DOI:10.1063/5.0240751

[17] G. Shukla, H.M. Abdullah, U. Schwingenschlögl. Nanoscale, **15** (37), 15161 (2023). DOI: 10.1039/d3nr04143c

[18] H. Jiang, T. Wang, Z. Zhang, F. Liu, R. Shi, B. Sheng, S. Sheng, W. Ge, P. Wang, B. Shen, B. Sun, P. Gao, L. Lindsay, X. Wang. Nature Commun., **15** (1), 9052 (2024). DOI:10.1038/s41467-024-53394-z

[19] J.M. Crowley J. Tahir-Kheli, W.A. Goddard. Phys. Chem. Lett., **7** (7), 1198 (2016).

[20] Á. Morales-García, R. Valero, F. Illas. J. Phys. Chem. C, **121** (34), 18862 (2017). DOI: 10.1021/acs.jpcc.7b07421

[21] A.L. Rosa, J. Neugebauer. Phys. Rev. B, **73** (20), 205346 (2006). DOI: 10.1103/PhysRevB.73.205346

[22] J. Heyd, G.E. Scuseria, M. Ernzerhof. J. Chem. Phys., **118** (18), 8207 (2003). DOI: 10.1063/1.1564060

[23] J.L. Lyons, C.G. Van de Walle. NPJ Comput. Mater., **3** (1), 12 (2017). DOI: 10.1038/s41524-017-0014-2

[24] D.O. Nielsen, C.G. Van de Walle, S.T. Pantelides, R.D. Schrimpf, D.M. Fleetwood, M.V. Fischetti. Phys. Rev. B, **108** (15), 155203 (2023). DOI: 10.1103/PhysRevB.108.155203
[25] J. Hubbard. Proc. Royal Soc. (London) A, **276** (1365), 238 (1963). DOI:10.1098/rspa.1963.0204
[26] F. Tran, P. Blaha. Phys. Rev. Lett., **102** (22), 226401 (2009). DOI: 10.1103/PhysRevLett.102.226401
[27] L.G. Ferreira, M. Marques, L.K. Teles. Phys. Rev. B, **78** (12), 125116 (2008). DOI: 10.1103/PhysRevB.78.125116
[28] P. Giannozzi, S. Baroni, N. Bonini, M. Calandra, R. Car, C. Cavazzoni, D. Ceresoli, G.L. Chiarotti, M. Cococcioni, I. Dabo, A.D. Corso, S. de Gironcoli, S. Fabris, G. Fratesi, R. Gebauer, U. Gerstmann, C. Gougoussis, A. Kokalj, M. Lazzeri, L. Martin-Samos, N. Marzari, F. Mauri, R. Mazzarello, S. Paolini, A. Pasquarello, L. Paulatto, C. Sbraccia, S. Scandolo, G. Sclauzero, A.P. Seitsonen, A. Smogunov, P. Umari, R.M. Wentzcovitch. J. Phys.: Condens. Matter, **21** (39), 395502 (2009). DOI: 10.1088/0953-8984/21/39/395502
[29] K. Shiraishi. J. Phys. Soc. Jpn., **59** (10), 3455 (1990). DOI:10.1143/JPSJ.59.3455
[30] C. Bungaro, K. Rapcewicz, J. Bernholc. Phys. Rev. B, **59** (15), 9771 (1999). DOI: 10.1103/PhysRevB.59.9771
[31] P. Kempisty, S. Krukowski, P. Strak, P.K. Sakowski. J. Appl. Phys., **106** (5), 054901 (2009). DOI: 10.1063/1.3204965
[32] B. Silvi, A. Savin. Nature, **371**, 683 (1994). DOI:10.1038/371683a0